Science Advances
AAAS

advances.sciencemag.org/cgi/content/full/6/26/eaaz4876/DC1

Supplementary Materials for

Climate impacts of a weakened Atlantic Meridional Overturning Circulation in a warming climate

Wei Liu*, Alexey V. Fedorov, Shang-Ping Xie, Shineng Hu

*Corresponding author. Email: wei.liu@ucr.edu

Published 26 June 2020, *Sci. Adv.* **6**, eaaz4876 (2020)
DOI: 10.1126/sciadv.aaz4876

This PDF file includes:

Figures

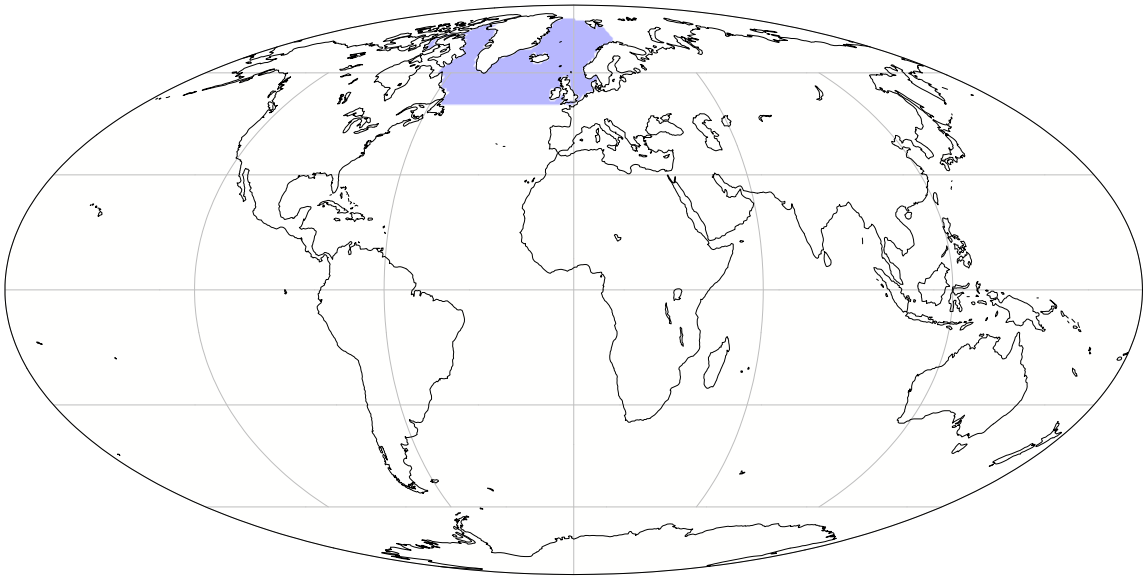

fig. S1. The region of freshwater removal. Freshwater is removed in the subpolar North Atlantic by altering virtual salt flux in CCSM4 in the region shaded light blue (See Materials and Methods). The southern boundary of this region is along 50°N, and the northern boundary is close to ~80°N, which separates the Arctic in the north along the Canadian Arctic Archipelago, the Fram Strait, and the western shelf of the Barents Sea. This region includes the areas of North Atlantic Deep Water formation to the south of the Iceland, in the Labrador Sea and in the Nordic Seas. Note that at times a northern part of this region is included in the Arctic Ocean.

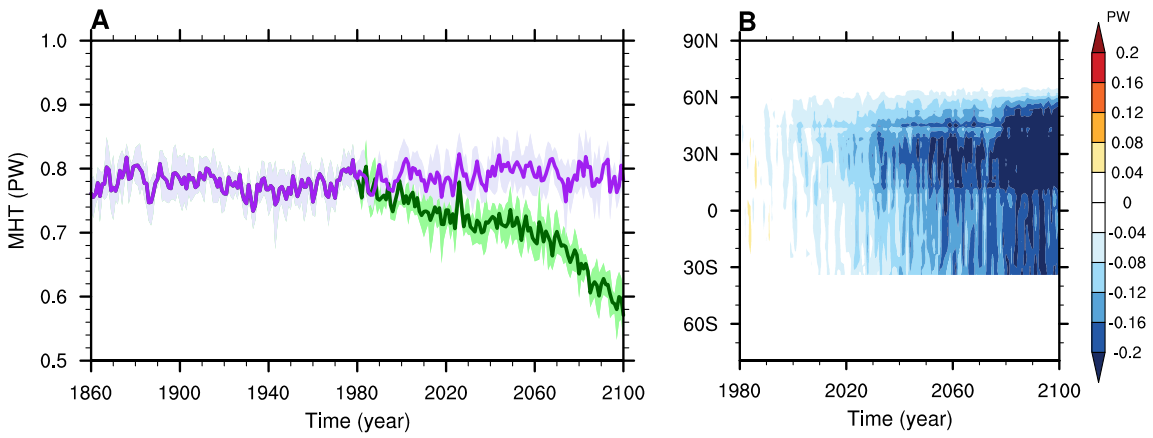

fig. S2. Atlantic meridional heat transport projections and AMOC impacts. (**A**) From 1860 to 1980, annual mean Atlantic northward heat transport at 55^{o}N is computed from CCSM4 historical simulation (purple: ensemble mean, light purple: ensemble spread). After 1980, annual mean Atlantic northward heat transport at 55^{o}N that follows CCSM4 historical and RCP8.5 simulations is shown as a green curve for ensemble mean with light green shading for ensemble spread. Annual mean Atlantic northward heat transport at 55^{o}N from the sensitivity experiment AMOC_fx (which starts after 1980) is shown as a purple curve for ensemble mean with light purple shading for ensemble spread. (**B**) Difference of annual mean Atlantic northward heat transports (blue shading, in PW) between the ensemble means of CCSM4 historical and RCP8.5 simulations and AMOC_fx during 1981-2100, which reveals the AMOC impacts on Atlantic meridional heat transport.

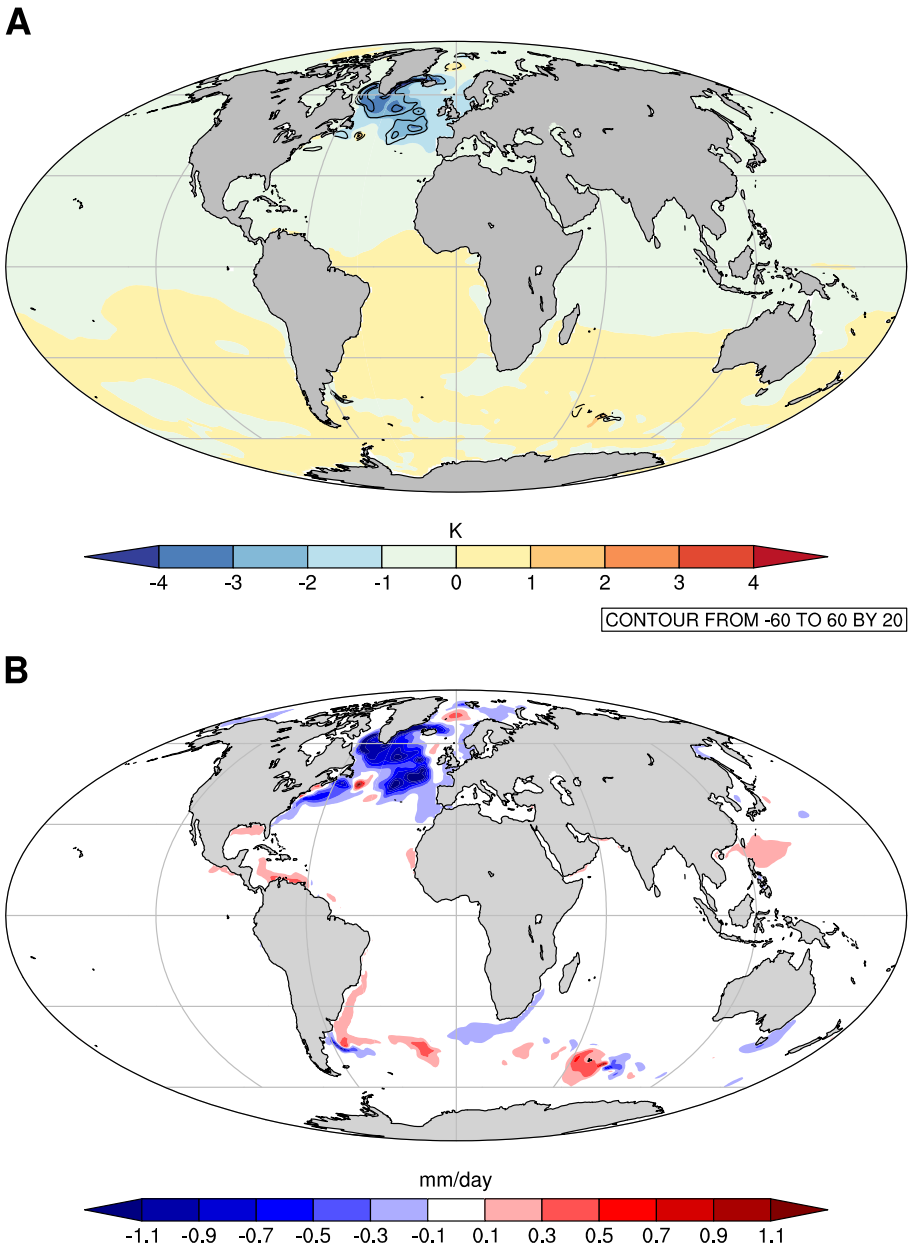

fig. S3. AMOC impacts on the projections of sea surface temperature, ocean surface heat flux and surface evaporation. (**A**) Differences of annual mean sea surface temperature (shading in K) and net downward ocean heat flux [contours, contour interval of 20 W/m^2; zero contours omitted and solid (dashed) contours used for positive (negative) values; positive values indicate ocean gains heat] during 2061-2080 between the ensemble means of CCSM4 RCP8.5 simulation and AMOC_fx (RCP8.5 minus AMOC_fx). (**B**) Difference of annual mean evaporation projections over the global ocean surface during 2061-2080 between the ensemble means of CCSM4 RCP8.5 simulation and AMOC_fx (RCP8.5 minus AMOC_fx).

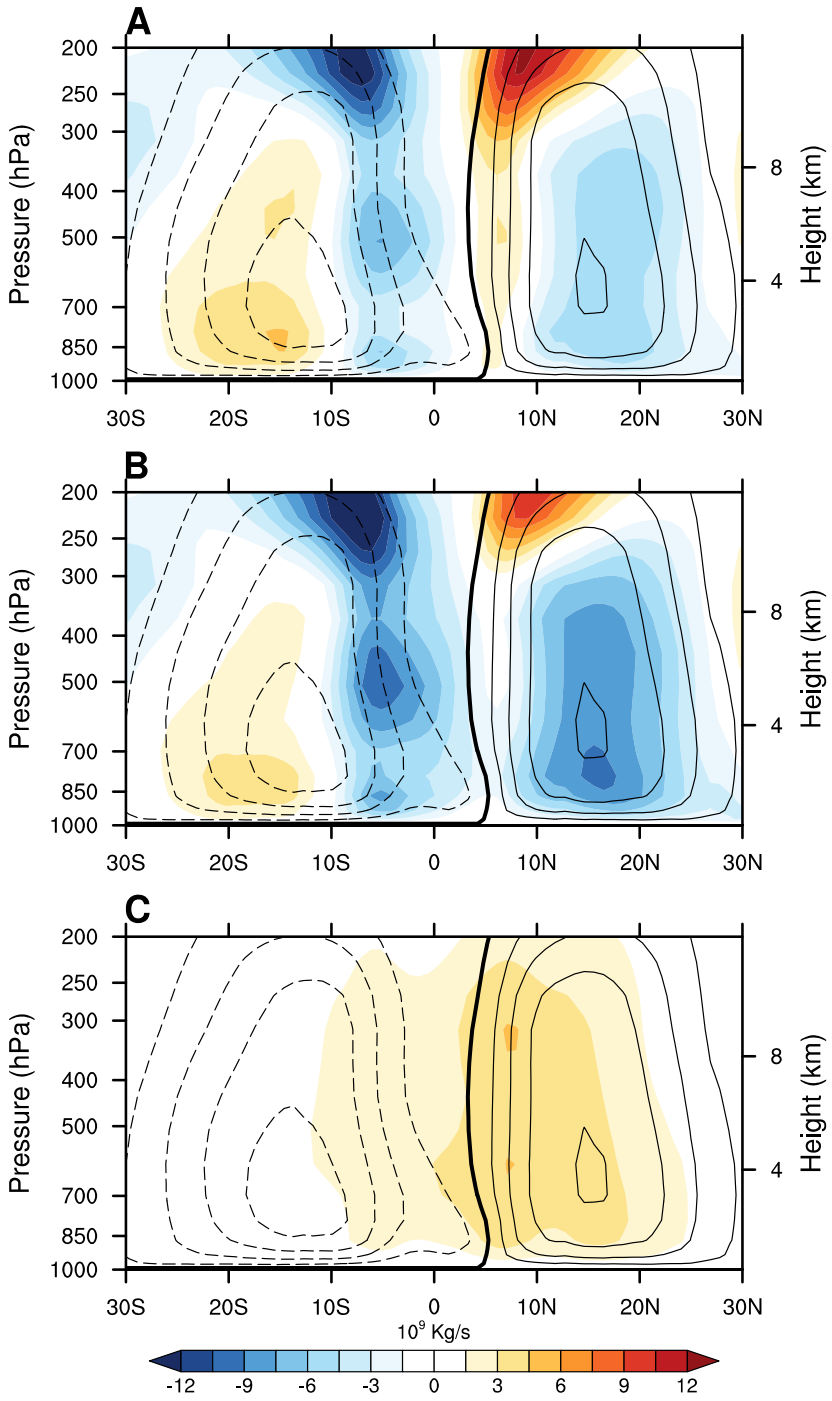

fig. S4. Hadley cell projections and AMOC impacts. Relative to 1961-1980, annual mean atmospheric mass streamfunction changes (shading in 10^9Kg/s) during 2061-2080 based on the ensemble means of (**A**) CCSM4 RCP8.5 simulation and (**B**) AMOC_fx. Panel (**C**) shows panel (**A**) minus panel (**B**). Contours in three panels show annual mean atmospheric mass streamfunction during 1961-1980 (contour interval of 2×10^{10}Kg/s).

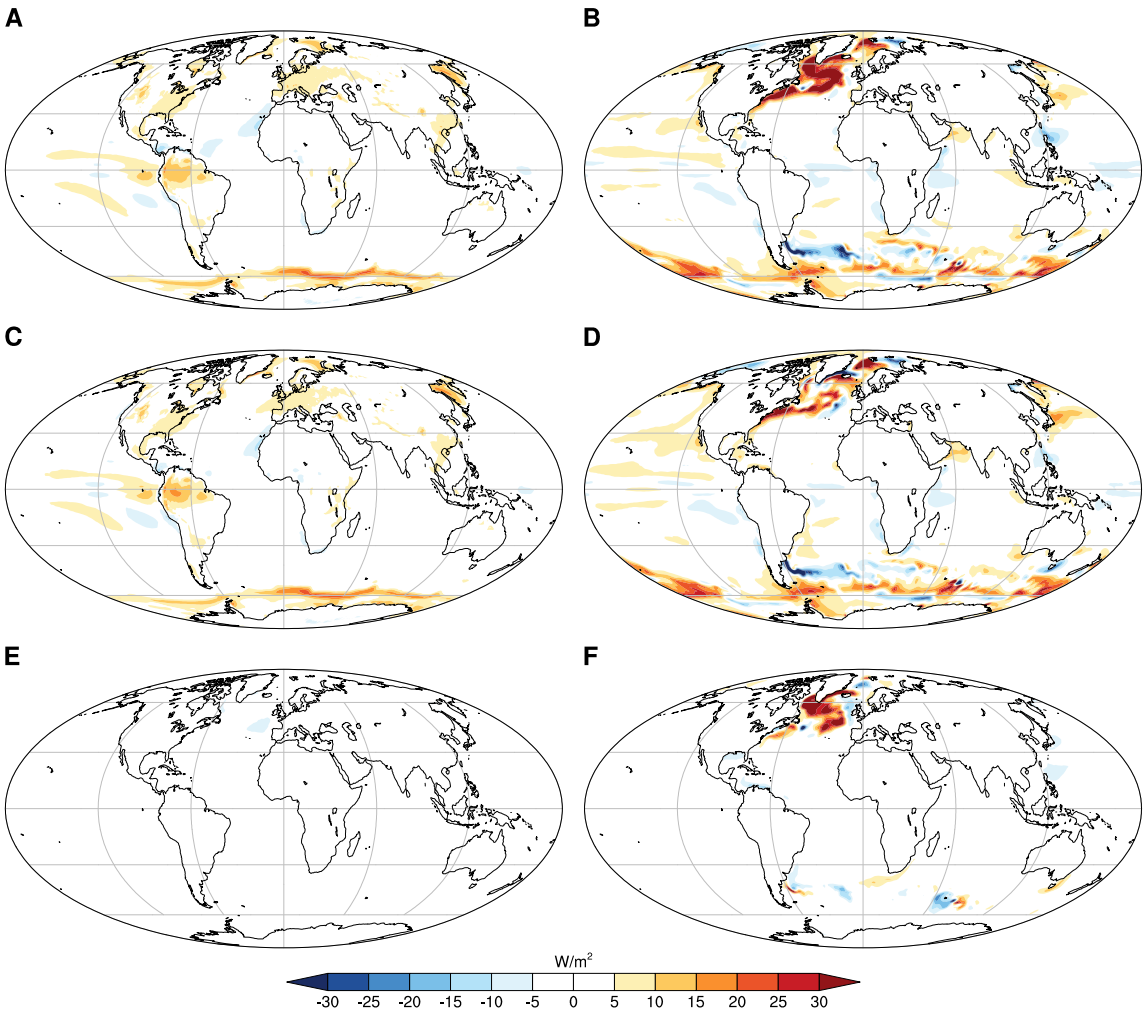

fig. S5. Projections of atmosphere energy fluxes across the TOA and Earth's surface and AMOC impacts. (left column) Relative to 1961-1980, annual mean atmosphere energy flux changes across the TOA (shading in W/m^2) during 2061-2080 based on the ensemble means of (**A**) CCSM4 RCP8.5 simulation and (**C**) AMOC_fx. Panel (**E**) shows panel (**A**) minus panel (**C**). (right column) Similar to left column but for annual mean atmosphere energy flux changes across Earth's surface. Panel (**F**) shows panel (**B**) minus panel (**D**). AMOC impacts on atmosphere energy flux changes across the TOA and Earth's surface are revealed in panels (**E**) and (**F**).

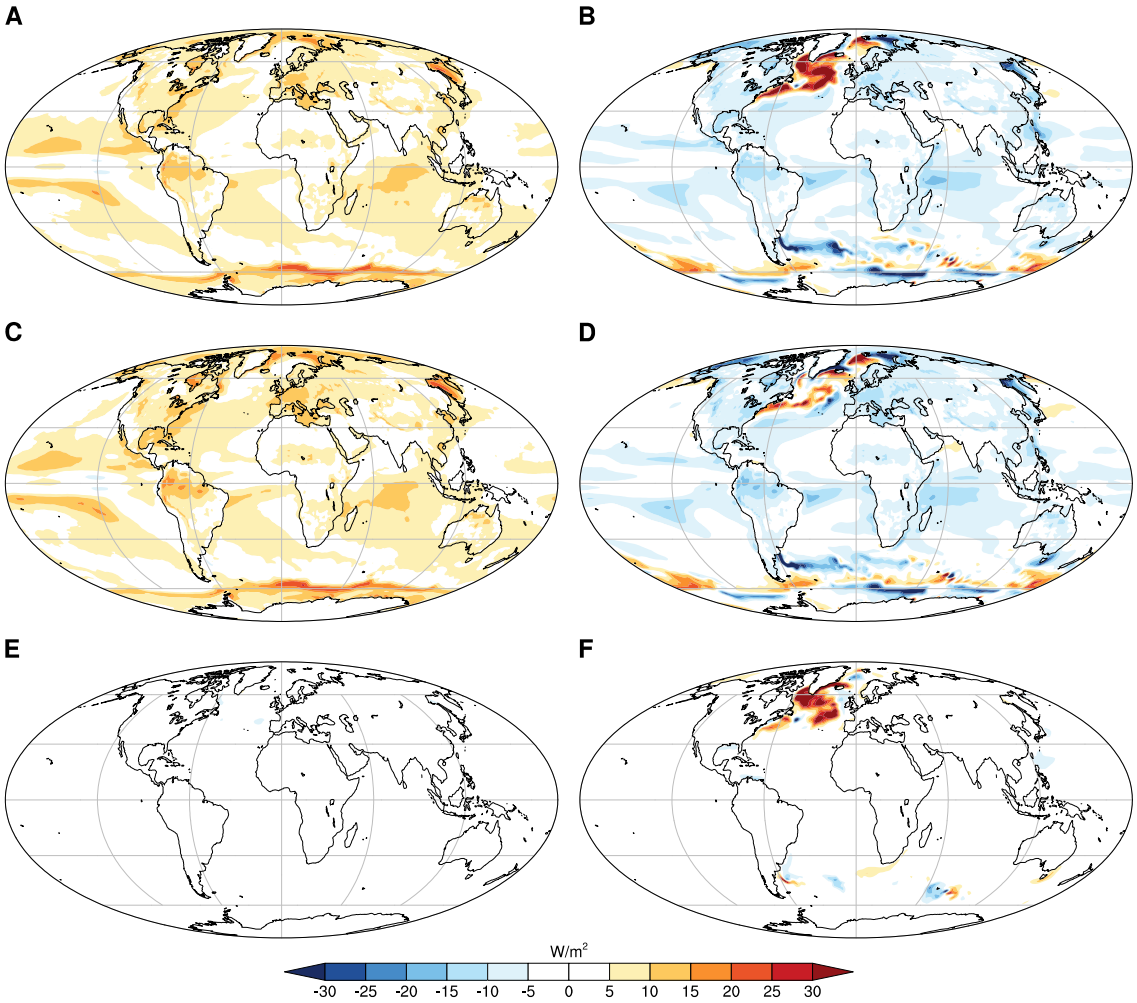

fig. S6. Projections of surface radiation and turbulent heat fluxes and AMOC impacts. (left column) Relative to 1961-1980, annual mean surface radiation (shortwave plus longwave) changes (shading in W/m^2) during 2061-2080 based on the ensemble means of (**A**) CCSM4 RCP8.5 simulation and (**C**) AMOC_fx. Panel (**E**) shows panel (**A**) minus panel (**C**). (right column) Similar to left column but for annual mean surface turbulent (sensible plus latent) heat flux changes. Panel (**F**) shows panel (**B**) minus panel (**D**). AMOC impacts on surface radiation and turbulent heat flux changes are revealed in panels (**E**) and (**F**).

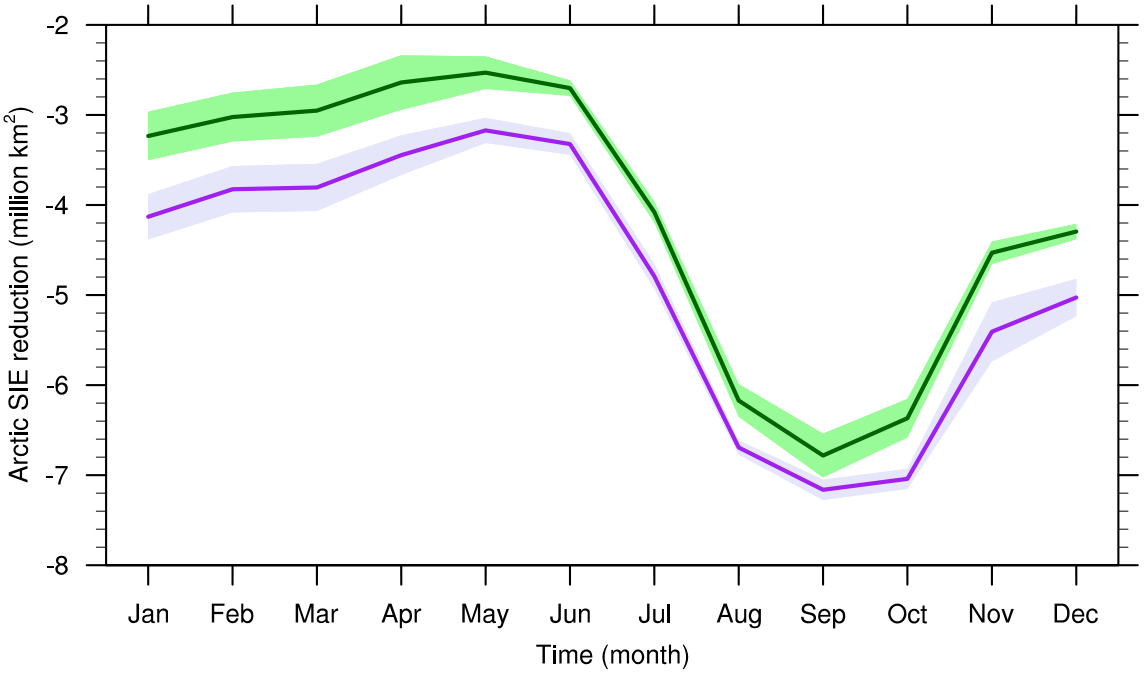

fig. S7. Arctic sea ice seasonal cycle projections. Relative to 1961-1980, seasonal Arctic sea ice extent changes during 2061-2080 between CCSM4 RCP8.5 simulation (green: ensemble mean; light green: ensemble spread) and AMOC_fx (purple: ensemble mean; light purple: ensemble spread).

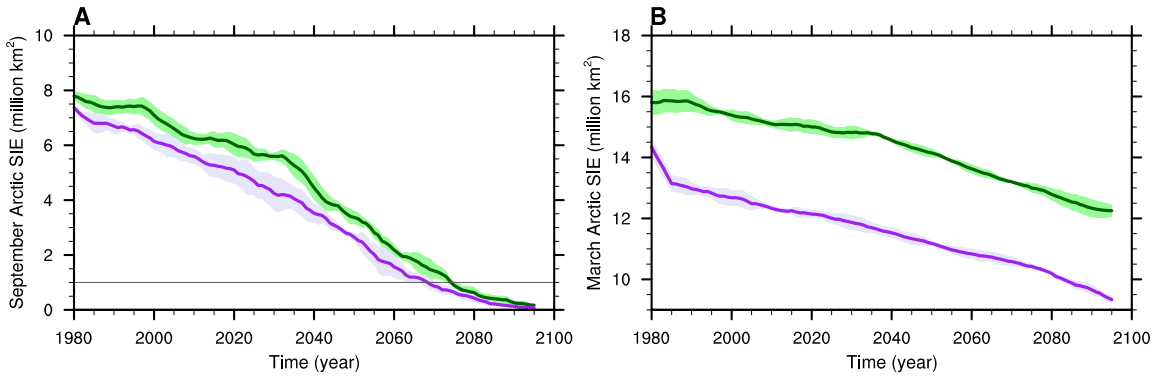

fig. S8. Evolution of Arctic sea ice excluding the sea ice within the freshwater removal region. Similar to Fig. 5A and B but excluding the sea ice within the freshwater removal region as shown in fig. S1.

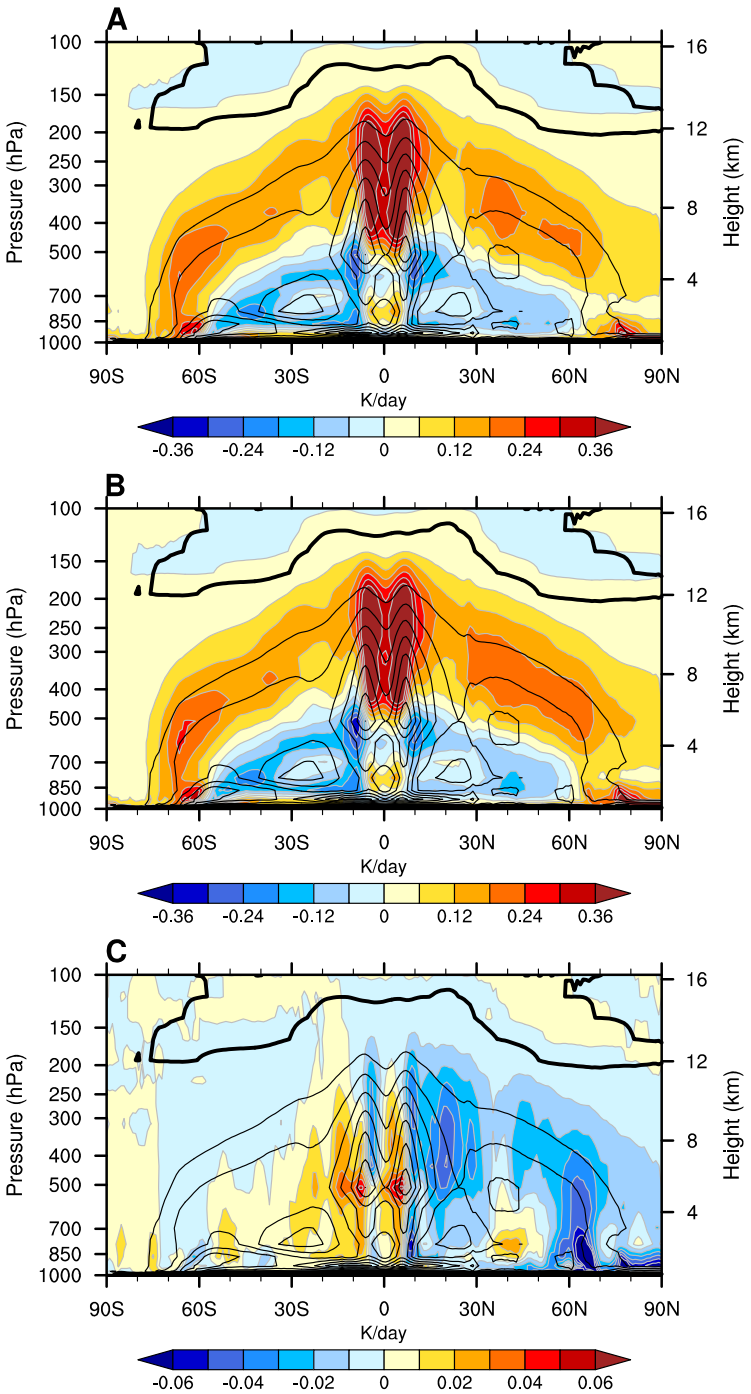

fig. S9. Projections of condensational heating rate and AMOC impacts. Relative to 1961-1980, annual and zonal mean condensational heating rate changes (K/day) during 2061-2080 based on the ensemble means of (**A**) CCSM4 RCP8.5 simulation and (**B**) AMOC_fx. Panel (**C**) shows panel (**A**) minus panel (**B**), revealing AMOC impacts on the projection of condensational heating rate. Contours in three panels show annual and zonal mean condensational heating rate during 1961-1980 (contour interval of 0.4 K/day and zero contours thickened).

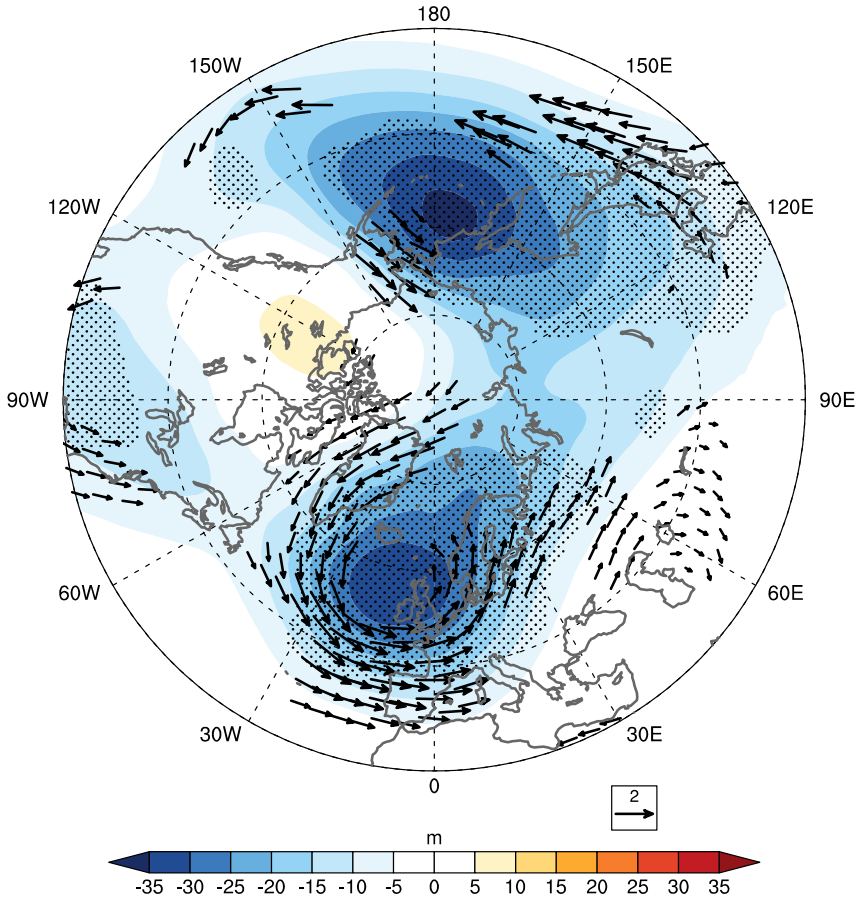

fig. S10. Projections of boreal wintertime midlatitude atmosphere circulation and AMOC impacts. Differences of DJF (December-January-February) 500 hPa geopotential heights (shading in m; stippling indicates where the differences are statistically significant at the 95% confidence level of Student's t-test) and 250 hPa winds (vector in m/s; only the differences that are statistically significant at the 95% confidence level of Student's t-test are plotted) to the north of 30^{o}N during 2061-2080 between the ensemble means of CCSM4 RCP8.5 simulation and AMOC_fx (RCP8.5 minus AMOC_fx).

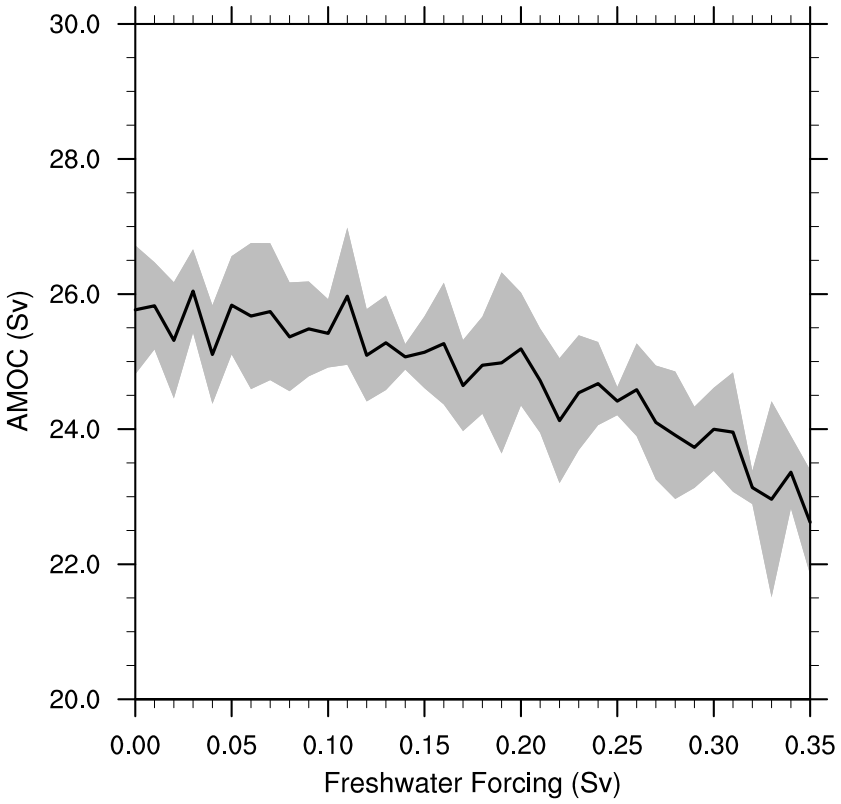

fig. S11. The sensitivity of AMOC strength to varying surface freshwater forcing. Starting from the CCSM4 preindustrial control run, the AMOC weakens under an increasing freshwater forcing in a hosing experiment (gray: ensemble spread; black: ensemble mean). Freshwater is added to the region shown in fig. S1 (See Materials and Methods for the details of freshwater forcing).

Table

table. S1. Heat budget analysis of the NAWH region. Differences of the terms in the heat budgets on the full-depth water column over the NAWH (Fig. 3) during 2061-2080 between the ensemble means of CCSM4 RCP8.5 simulation and AMOC_fx (RCP8.5 minus AMOC_fx). See Materials and Methods for the notations of the heat budget terms.

Heat budget term	Difference (PW)
TEN	-0.031
SHF	0.074
D	-0.002
$-\Delta OHT$	-0.103
OHT(S)	-0.165
OHT(N)	-0.062
OHT_{Eul} (S)	-0.153
OHT_{ed+sub} (S)	-0.012
OHT_{ov}	-0.124
OHT_{az}	-0.029
OHT_{Eul} (N)	-0.079
OHT_{ed+sub} (N)	0.017